RSC Advances

PAPER

View Article Online
View Journal | View Issue

Cite this: *RSC Adv.*, 2020, **10**, 14161

High antiviral activity of mercaptoethane sulfonate functionalized Te/BSA nanostars against arterivirus and coronavirus†

Yanrong Zhou,‡[abc] Xiaohan Jiang,‡[ad] Ting Tong,[ade] Liurong Fang,[abc] Yuan Wu,[ad] Jiangong Liang *[ade] and Shaobo Xiao *[abc]

Heparan sulfate (HS) is a kind of cellular adhesion receptor that mediates the attachment and internalization of virus infection. Herein, to mimic the cell surface receptor, mercaptoethane sulfonate (MES), an analogue of HS, was used as the surface modifier to synthesize bovine serum albumin (BSA)-coated tellurium nanoparticles (Te/BSA NPs) with a unique triangular star shape (Te/BSA nanostars). Using porcine reproductive and respiratory syndrome virus (PRRSV), which utilizes HS as a cellular receptor, as a model of arterivirus, we found that Te/BSA nanostars suppressed virus infection mainly by inhibiting the virus internalization process. Interestingly, Te/BSA nanostars exhibited much higher antiviral activity than the spherical Te/BSA NPs (Te/BSA nanospheres), the Te/BSA NPs were synthesized with GSH as a substitute of MES, suggesting that both MES modification and the novel shapes of Te/BSA NPs enhance their antiviral activity. Finally, the antiviral effect of Te/BSA nanostars on porcine epidemic diarrhea virus (PEDV), a model of coronavirus, was also demonstrated, indicating the potential broad-spectrum antiviral property of Te/BSA nanostars.

Received 13th February 2020
Accepted 31st March 2020

DOI: 10.1039/d0ra01387k

rsc.li/rsc-advances

1. Introduction

In recent years, functionalized nanomaterials have been widely used in the biomedical field because of their unique physical and chemical properties.[1] Among them, many are applied in antiviral research,[2] such as macromolecular copolymers (peptide–polymer conjugates), fullerene-polyglycerol sulfates, metal nanoparticles (NPs) (*e.g.*, AgNPs and AuNPs) and quantum dots.[3–10] However, the complexity of synthetic methods (*e.g.*, macromolecular copolymers), the cytotoxicity of degradation products (*e.g.*, precious metal NPs) and the poor stability (*e.g.*, NPs with sheet or fiber structures) limit the application of most antiviral NPs to some extent.[4,11–13] Therefore, it is extremely necessary to develop nanomaterials with good biocompatibility and high stability using a simple and fast synthetic method.

An increasing number of antiviral nanomaterials have been developed by interfering with the interaction between virus and its associated cell receptor to achieve broad-spectrum efficacy.[14,15] Heparan sulfate proteoglycans (HSPGs) are reported to act as receptors of many viruses, such as dengue virus, human cytomegalovirus (HCMV), human immunodeficiency virus (HIV), respiratory syncytial virus (RSV), herpes simplex virus (HSV), filoviruses and human papillomavirus (HPV).[16] Heparan sulfates (HS), an important constituent of HSPG, are structurally similar to heparin. Hence, it is a novel strategy to construct antiviral nanomaterials by mimicking HS.[17–19] Inspired by this idea, mercaptoethane sulfonate (MES), an analogue of HS, was found to significantly enhance the antiviral activity of various NPs.[17,20,21]

Viruses and bacteria vary in shapes, ranging from sphere to filament. Non-spherical shapes increase their ability to escape immune responses.[22] As for nanomaterials, non-spherical nanomaterials are likely to exhibit superior antiviral and/or antibacterial properties relative to nanospheres with a similar size.[23–28] For example, the nanosheet structure of graphene oxide was shown to be important for its antiviral properties against pseudorabies virus (PRV) and PEDV;[29] bioprotective nanofibrous membranes (RNMs) were reported to have high bactericidal and viricidal efficacy.[30] However, the majority of currently reported antiviral nanomaterials exist in a spherical form,[31,32] suggesting the possibility to enhance the functional

[a]*State Key Laboratory of Agricultural Microbiology, Huazhong Agricultural University, Wuhan 430070, P. R. China. E-mail: liangjg@mail.hzau.edu.cn; vet@mail.hzau.edu.cn; Fax: +86-27-8728-2608; Tel: +86-27-8728-6884*

[b]*College of Veterinary Medicine, Huazhong Agricultural University, Wuhan 430070, P. R. China*

[c]*The Cooperative Innovation Center for Sustainable Pig Production, Wuhan 430070, P. R. China*

[d]*College of Science, Huazhong Agricultural University, Wuhan 430070, P. R. China*

[e]*College of Resources and Environment, Huazhong Agricultural University, Wuhan 430070, P. R. China*

† Electronic supplementary information (ESI) available. See DOI: 10.1039/d0ra01387k

‡ These authors contributed equally to this work.

properties of nanomaterials through reasonable and effective control of their morphology.

Porcine reproductive and respiratory syndrome (PRRS) virus (PRRSV), a single-stranded, positive-strand RNA virus classified within the *Arteriviridae* family, is the causative agent of PRRS. PRRS, mainly characterized by dyspnea in piglets and growing pigs and reproductive failure in sows, is an important infectious disease with an adverse effect on the global pig industry for nearly 30 years.[33] Vaccination is the common way to control PRRSV infection. Unfortunately, most commercial vaccines fail to provide effective prevention and control against PRRS.[34,35] Currently, antiviral drug therapy has been regarded as a novel and potent tool to combat virus infection.

Considering that HS is a potential cellular receptor for PRRSV infection,[36] we attempted to synthesize antiviral NPs with MES as the surface modifier and investigate their antiviral potential using PRRSV as a model of arterivirus. The MES-functionalized Te/BSA NPs with a novel triangular star shape (Te/BSA nanostars) was prepared and demonstrated as a potent antagonist against PRRSV. Further comparing experiments indicated that MES could modify the morphology to improve the antiviral property of Te/BSA NPs, prompting the potential correlation between the antiviral activity and the novel triangular star shape of NPs. Moreover, we found that Te/BSA nanostars mainly repressed the internalization stage of PRRSV infection, coincident with the function of MES as a mimic of cellular receptor HS. Finally, Te/BSA nanostars also exhibited inhibitory effect on the infection of porcine epidemic diarrhea virus (PEDV), a model of coronavirus using HS as an attachment factor as well, indicating the potential antiviral property of Te/BSA nanostars against the other coronaviruses, such as 2019 novel coronavirus (2019-nCoV), severe acute respiratory syndrome coronavirus (SARS-CoV) and Middle East respiratory syndrome coronavirus (MERS-CoV).[37,38] Overall, the Te/BSA nanostar is a potential nanomaterial for the further development of safe and effective antiviral drugs.

2. Results and discussion

2.1 Characterization of Te/BSA nanostars

Previously, we have prepared Te/BSA nanospheres using sodium tellurite, BSA, and glutathione (GSH) as precursors. Here, Te/BSA nanostars were synthesized by modification using MES to replace GSH as the modifier.[39] The transmission electron microscopy (TEM) image (Fig. 1a) showed that the as-prepared Te/BSA nanostars had a triangular star shape, which was obviously different from that of the spherical Te/BSA nanospheres,[39] indicating that MES not only acts as a reductant, but also remarkably modifies the morphology of NPs, which is similar to the role of ascorbic acid in the synthesis of BSA/Au nanostars.[40] The TEM image also showed the good dispersion of Te/BSA nanostars, with an average size of 57 ± 7.6 nm, which was basically consistent with the result of dynamic light scattering (DLS; Fig. 1b). In Fig. 1c, the UV-vis spectrum of the Te/BSA nanostars displayed a strong absorption peak near 277 nm, which is due to the $\pi \rightarrow \pi^*$ electron transition of C=C and the $n \rightarrow \pi^*$ of C=O band.[41–43] As

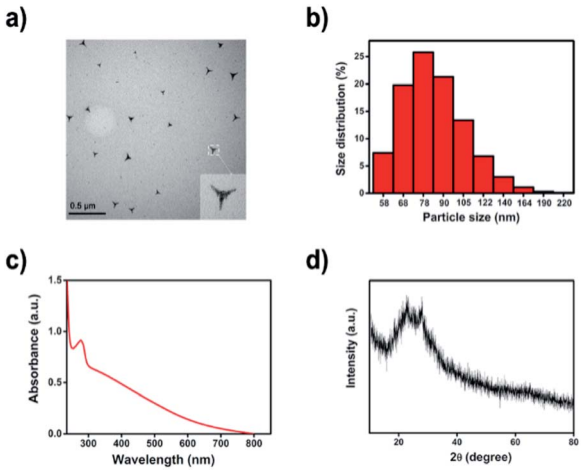

Fig. 1 (a) The TEM image of Te/BSA nanostars. (b) Hydrodynamic diameter distribution of Te/BSA nanostars from DLS. (c) UV-vis absorption spectrum of Te/BSA nanostars. (d) The XRD patterns of Te/BSA nanostars.

illustrated in Fig. 1d, the XRD patterns of Te/BSA nanostars showed two strong absorption peaks between 20–30°, indicating the presence of (100, 101) facets of Te, which consist with the standard literature value (JCPDF no. 36-1452).[44]

The FT-IR spectra of Te/BSA nanostars and MES, one of the precursors of Te/BSA nanostars, were collected in the transmission mode between 500 and 4000 cm^{-1}. As shown in Fig. S1,† the characteristic $-SO_3$ vibrational peak could be clearly seen in the FT-IR spectra of MES.[45] The small peak at 2561 cm^{-1}, corresponding to the stretching vibration mode of –SH in MES, disappeared in the FT-IR spectra of Te/BSA nanostars, providing strong evidence that the sulfur atom in the thiol group of MES was anchored on the surface of Te.[46] Moreover, no remarkable difference was observed in the stretching vibration band of O=S=O between Te/BSA nanostars and MES.

Additionally, the X-ray photoelectron spectroscopy (XPS) analysis of Te/BSA nanostars showed five distinct peaks at 163.9, 284.8, 399.8, 531.6, and 576.1 eV, which correspond to S 2p, C 1s, N 1s, O 1s, and Te 3d, respectively (Fig. 2a). The XPS spectrum of C 1s (Fig. 2b) might indicate the existence of four groups, including C=O (287.9 eV), C–O (285.7 eV), C–N (284.9 eV) and C–C (284.3 eV).[47,48] In the XPS spectrum of N 1s, there were three typical peaks at 400.8, 399.6, and 399.3 eV, which are assigned to $N-(C)_3$, C–N–C, and C=N–C, respectively (Fig. 2c).[49–51] In Fig. 2d, the XPS spectrum of S 2p revealed the existence of sulfur in two major oxidation states. The two peaks at 165.2 and 163.9 eV indicated the presence of thiol group (S–H) ($2p_{3/2}$ and $2p_{1/2}$), and the other two peaks at 169.5 and 168.7 eV are attributed to the sulfonate group ($2p_{3/2}$ and $2p_{1/2}$).[18,51] In Fig. 2e, the Te 3d core level spectrum showed the peaks at 583.6 and 573.1 eV, which separately correspond to Te $3d_{3/2}$ and Te $3d_{5/2}$, while the other two peaks at 586.5 and 576.4 eV are attributed to the oxidation state of Te.[52–54]

Then we perform the thermogravimetric analysis under a nitrogen atmosphere at 30–700 °C.[55] Fig. S2† shows the relationship between weight loss (%) and temperature change of

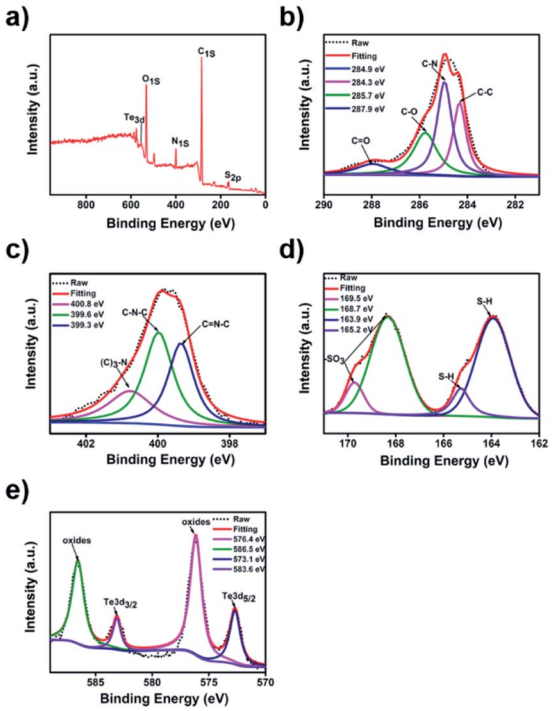

Fig. 2 XPS spectra of Te/BSA nanostars (a), C 1s (b), N 1s (c), S 2p (d) and Te 3d (e).

Te/BSA nanostars. An initial weight loss of about 10% was observed in the 50–100 °C range, which was attributed to the water molecules adsorbed on the surface of nanostars. A further loss of about 48% in weight was detected in the temperature range of 200–500 °C. This loss occurred in two steps: ~35% of the weight was lost in the range of 200–330 °C and ~13% in the range of 320–550 °C, which was attributed to the removal of MES that was chemically bonded to the surface of Te core.[17]

2.2 Cytotoxicity assays

The potential cytotoxicity of Te/BSA nanostars on MARC-145 cells was evaluated at 12, 24, 36 or 48 h post incubation. The results of MTT assay indicated that the percent of living MARC-145 cells was higher than 90% under the treatment with 15.0 μg mL^{-1} of Te/BSA nanostars for 48 h (Fig. 3). Thus, 15.0 μg mL^{-1} was chosen as the concentration of Te/BSA nanostars for the subsequent experiments in MARC-145 cells.

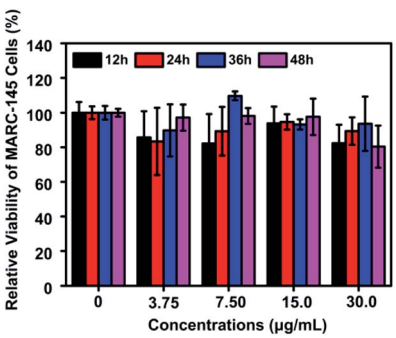

Fig. 3 Cytotoxicity of Te/BSA nanostars as detected by MTT assay. All values were normalized to the control group (without Te/BSA nanostars exposure).

2.3 Te/BSA nanostars exhibit inhibitory effect on PRRSV infection

Firstly, MARC-145 cells were treated or mock-treated with 15.0 μg mL^{-1} of Te/BSA nanostars, and then the titers of intracellular and supernatant PRRSV were separately examined by plaque assay. In Fig. 4a and b, it can be seen that Te/BSA nanostars decreased the amount of PRRSV in both intracellular and supernatant samples. Then the antiviral effect of Te/BSA nanostars on PRRSV (MOI = 1.0) was further investigated through western blot assay. The expression level of PRRSV nsp2, the largest viral protein that is key for PRRSV replication,[56] was detected. As shown in Fig. 4c, the expression level of PRRSV nsp2 was obviously down-regulated under the treatment of Te/BSA nanostars, prompting that Te/BSA nanostars could inhibit the expression of PRRSV proteins.

The indirect immunofluorescence assay (IFA) with antibodies against virus is considered as a useful diagnostic technique. Here, IFA was used to further verify the potential antiviral activity of Te/BSA nanostars against PRRSV (MOI = 1.0). As evident from Fig. 4d, the green fluorescence signal was dramatically decreased in cells incubated with Te/BSA nanostars (the third row) relative to the control group (the second row), demonstrating the predominant antiviral activity of Te/BSA nanostars against PRRSV, which well supported the results of plaque assay and western blot assay.

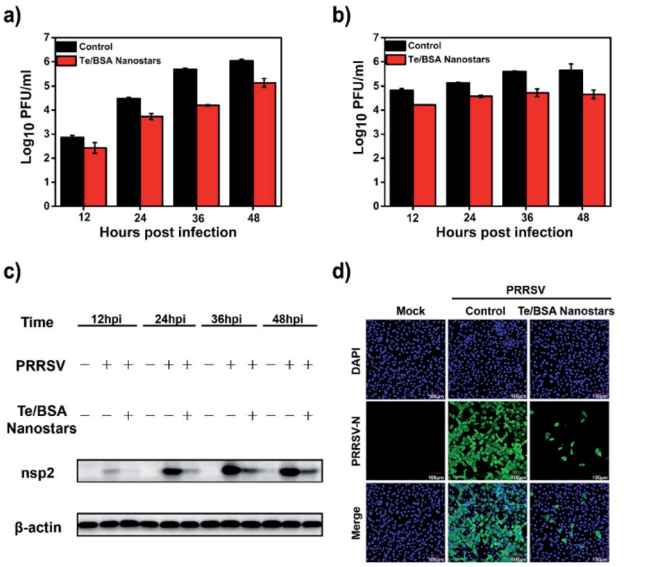

Fig. 4 The titers of supernatant PRRSV (a) and intracellular PRRSV (b) as evaluated by plaque assay. (c) The effect of Te/BSA nanostars (15.0 μg mL^{-1}) on the expression level of PRRSV nsp2 as evaluated by western blot assay. (d) The influence of Te/BSA nanostars (15.0 μg mL^{-1}) on PRRSV proliferation as evaluated by indirect immunofluorescence assay.

2.4 Te/BSA nanostars inhibit adsorption, internalization and replication of PRRSV

Many antiviral NPs have been reported to inhibit virus infection by targeting the process of virus infecting host cells.[57] The virus propagation cycle mainly includes four steps: adsorption, internalization, replication and virion release.[58,59] In order to explore the specific step(s) targeted by Te/BSA nanostars to inhibit proliferation of PRRSV, a plaque formation assay was performed to test the influence of Te/BSA nanostars on PRRSV adsorption, then we found that the Te/BSA nanostars slightly inhibited PRRSV adsorption (Fig. 5a). In addition, the effect of Te/BSA nanostars on the internalization process of PRRSV infection was detected. In Fig. 5b, it can be seen that the plaque number was significantly reduced when treated with Te/BSA nanostars, suggesting that Te/BSA nanostars inhibit the PRRSV proliferation mainly through targeting its internalization. Then the influence of Te/BSA nanostars on PRRSV replication was tested by evaluating the amount of PRRSV negative-sense RNA. As indicated in Fig. 5c, when compared with the control group treated with DMEM, there was a slight decrease in PRRSV negative-sense RNA level in cells incubated with Te/BSA nanostars, indicating that Te/BSA nanostars have a moderate inhibition effect on PRRSV replication. For the final step in the propagation cycle, the virion release of PRRSV, there was no significant difference in virus titer between Te/BSA nanostar-incubated and DMEM-incubated groups (Fig. 5d and e), prompting that Te/BSA nanostars have no influence on the virion release of PRRSV.

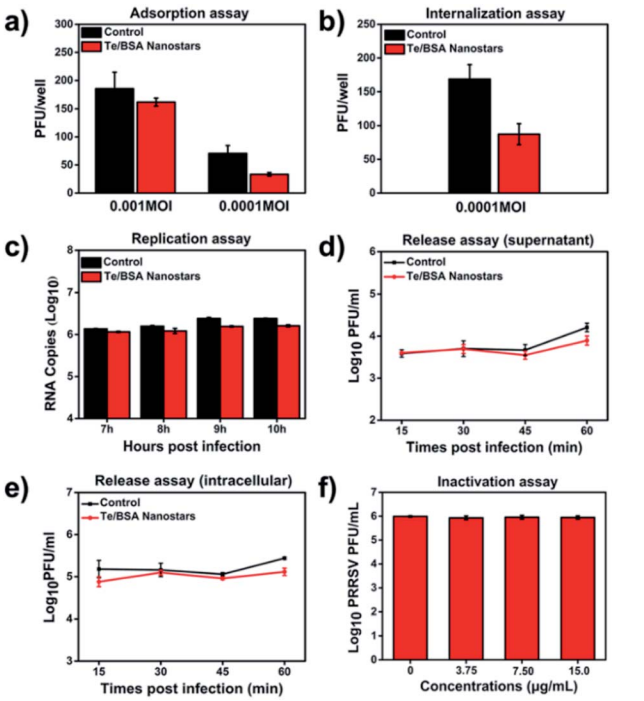

Fig. 5 The effect of Te/BSA nanostars on adsorption (a), internalization (b), replication (c) and virion release (d and e) of PRRSV. The titers of supernatant PRRSV (d) and intracellular PRRSV (e). (f) The direct inactivation effect of Te/BSA nanostars on PRRSV.

The mechanism by which Te/BSA nanostars inhibit PRRSV proliferation was further examined by evaluating the potential direct inactivation effect of Te/BSA nanostars on PRRSV. In Fig. 5f, it can be seen that Te/BSA nanostars had no direct inactivation effect on PRRSV. Besides the above potential aspects targeted by antiviral NPs for antiviral activity, the direct effect of Te/BSA nanostars on host cells, which may alter the cell susceptibility and permissivity to viral infection, was also explored here. We found that the effect of Te/BSA nanostars on cells slightly contributed to the anti-PRRSV activity of Te/BSA nanostars (Fig. S3†), implying that Te/BSA nanostars have potential prophylactic effect against PRRSV infection to some extent.

2.5 Te/BSA nanostars decrease PRRSV-induced production of reactive oxygen species (ROS)

Virus infection poses a great threat to human and animal health, even more serious, some commercial antiviral drugs have led to the rapid emergence of drug-resistant variants.[60] Therefore, it is urgent to develop antiviral drugs against the factors of virus-infected host cells rather than viral components themselves to decrease the number of drug-resistant variants.[61] Virus infection produces high concentrations of ROS, a series of reactive oxygen species generated by aerobic cells during metabolic processes. ROS in a certain concentration range could induce apoptosis or even necrosis through cellular oxidative stress.[62] Previous studies have indicated that reducing ROS levels through ROS inhibitors can inhibit virus reproduction, which prompts us that ROS is a potential novel target for antiviral drug development.[63–66] Hence, we tried to explore whether Te/BSA nanostars achieve antiviral activity by regulating ROS level.

DCF was used to analyze the production of ROS. In Fig. 6a, the results of flow cytometry revealed that PRRSV increased the level of ROS in MARC-145 cells, while Te/BSA nanostars significantly decreased PRRSV-induced ROS production. Consistently, the fluorescence images also illustrated that PRRSV-induced ROS level (green fluorescence signal) was obviously downregulated by Te/BSA nanostars (Fig. 6b). These results indicated that Te/BSA nanostars might restrict PRRSV propagation through inhibiting PRRSV-induced ROS generation.

2.6 MES modification enhances the antiviral activity of Te/BSA nanostars on PRRSV

Baram-Pinto *et al.* reported that unmodified gold nanoparticles (Au NPs) are ineffective in inhibiting the infection of HSV-1, while Au NPs capped with MES (Au-MES NPs) have excellent anti-HSV-1 activity.[18] To investigate whether MES modification also contributes to the antiviral activity of Te/BSA nanostars, the antiviral potential of Te/BSA nanostars was compared with that of Te/BSA nanospheres, which was modified with GSH rather than MES. First, the cytotoxicity of Te/BSA nanospheres (0, 7.50, 15.0, 30.0, 60.0, 80.0 μg mL^{-1}) on MARC-145 cells was evaluated (Fig. S4†). Then the anti-PRRSV abilities of Te/BSA nanostars or Te/BSA nanospheres were detected by the indirect immunofluorescence assay at 36 hpi (hours post infection). As evident from

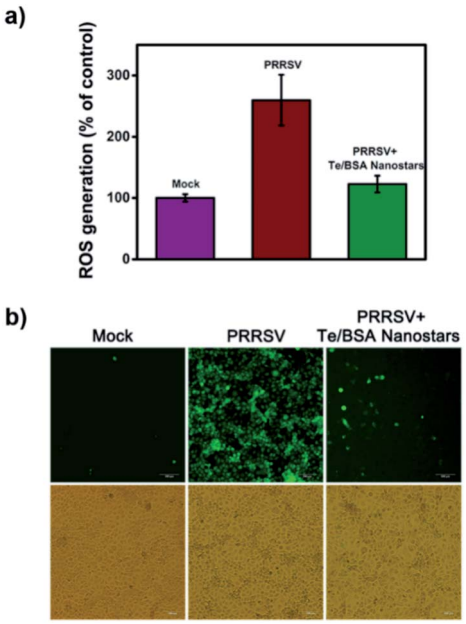

Fig. 6 Te/BSA nanostars decrease PRRSV-induced production of reactive oxygen species (ROS). MARC-145 cells were infected or mock infected with PRRSV (1.0 MOI) in the absence or presence of Te/BSA nanostars at the concentration of 15.0 μg mL^{-1}. (a) Relative quantitative evaluation of ROS levels through flow cytometry. (b) ROS levels illustrated by the fluorescence images obtained by an inverted fluorescence microscope.

Fig. 7, the green fluorescence signal (PRRSV N protein) was dramatically decreased in cells treated with Te/BSA nanostars (the third column) relative to the control group (the second column), while no obvious difference was observed in green fluorescence signal of PRRSV N protein between the group treated with Te/BSA nanospheres (the fourth column) and the control group (the second column), suggesting that the Te/BSA nanostars had excellent antiviral properties against PRRSV, but not the Te/BSA nanospheres. The results demonstrated that MES modification could significantly increase the anti-PRRSV ability of Te/BSA nanostars.

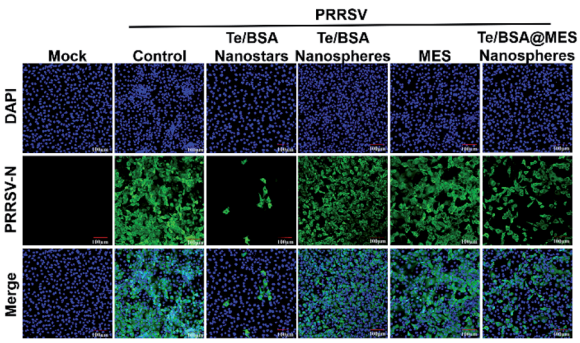

Fig. 7 The effect of Te/BSA nanostars (15.0 μg mL^{-1}), Te/BSA nanospheres (15.0 μg mL^{-1}), Te/BSA@MES nanospheres (15.0 μg mL^{-1}) and MES (1.50 mmol L^{-1}) on PRRSV proliferation as evaluated by indirect immunofluorescence assay.

To test whether the existence of free MES contributes to the anti-PRRSV activity of Te/BSA nanostars, the cytotoxicity of MES on MARC-145 cells was detected, and then 1.50 mmol L^{-1} (246 μg mL^{-1}) of MES was chosen for further experiment (Fig. S5†). The antiviral effect of MES on PRRSV was explored through indirect immunofluorescence assay. We found that no obvious change was observed in the number of PRRSV-infected cells when incubated with MES (the fifth column), while the number of PRRSV-infected cells in Te/BSA nanostar-treated group (the third column) was significantly smaller than that in the control group (the second column) (Fig. 7). The results showed that MES itself had no noticeable antiviral effect on PRRSV, but MES modification could remarkably increase the antiviral ability of Te/BSA nanostars. This is in line with a previous study reporting that MES has no inhibitory effect on the infection of HSV-1, but the MES functional groups modified on the surfaces of Au NPs give antiviral properties to Au-MES NPs.[18] The inefficacy of MES as an antiviral agent can be attributed to its free rotation, which limits the binding affinity of sulfonate groups to viral proteins. However, when capped on the surface of NPs, MES is converted from a weakly binding small molecule into a multivalent biologically effective compound, thereby resulting in an increase of the local concentration of MES and the subsequent enhanced interactions between MES and viruses.[67,68]

2.7 Potential broad antiviral spectrum of Te/BSA nanostars

Porcine epidemic diarrhea virus (PEDV), a model of coronavirus, is the causative agent of PED, an economically predominant swine disease.[69] A previous study has reported that heparan sulfate is an attachment factor of PEDV,[70] and we hypothesize that Te/BSA nanostars also exhibit antiviral ability against PEDV. To test this hypothesis, we first evaluated the cytotoxicity of Te/BSA nanostars on Vero cells. As shown in Fig. S6,† the percent of living cells was above 90% under the treatment with 30.0 μg mL^{-1} of Te/BSA nanostars for 24 h. Thus, 15.0 and 30.0 μg mL^{-1} of Te/BSA nanostars were chosen as the concentrations for subsequent antiviral experiments in Vero cells.

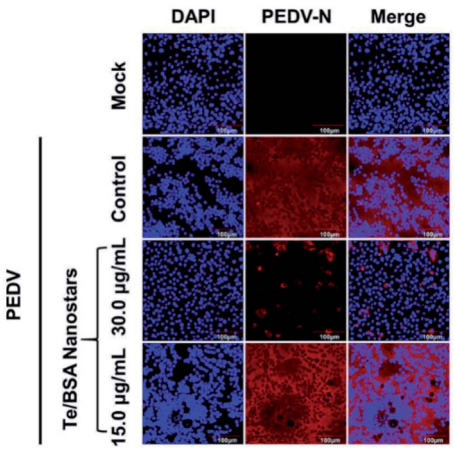

Fig. 8 The antiviral effect of Te/BSA nanostars on PEDV in Vero cells as evaluated by indirect immunofluorescence assay.

The antiviral activity of Te/BSA nanostars against PEDV was explored by indirect immunofluorescence assay. As shown in Fig. 8, the number of PEDV-infected cells (red fluorescence signal labeled by antibody against PEDV N protein) was significantly decreased by Te/BSA nanostars at the concentration of 30.0 μg mL^{-1}, but not at 15.0 μg mL^{-1}, indicating that Te/BSA nanostars inhibited PEDV propagation in a dose-dependent manner. As heparan sulfate also accounts for the infection of many other viruses, such as HIV, HCMV, HSV, HPV, RSV and dengue virus,[70] Te/BSA nanostars may act as a generic antiviral agent in addition to PRRSV.

Several studies have demonstrated that the non-spherical morphology of nanomaterials is beneficial for the antiviral and/or antibacterial potential.[23–27] In this paper, we found that the usage of MES instead of GSH to prepare Te/BSA nanostars led to the change of morphology from spherical shape to special triangular star shape, and simultaneously, the upregulation of their antiviral activity. To investigate whether the star shape enhances the anti-PRRSV ability of Te/BSA NPs, Te/BSA@MES nanospheres were synthesized with GSH as described for Te/BSA nanospheres and then MES was used to replace GSH as a modifier to synthesize Te/BSA@MES nanospheres. A comparison analysis revealed that the Te/BSA@MES nanospheres had higher antiviral activity than Te/BSA nanostars (Fig. 7), indicating that the novel star shape affects the antiviral potential of NPs, which was also demonstrated by Kwon *et al.*[71] Furthermore, we speculate that the novel triangular star shape of Te/BSA nanostars can benefit their penetration into cytoplasm, thereby giving rise to more excellent antiviral activity of Te/BSA nanostars on PRRSV. Thus, FITC was conjugated to both Te/BSA nanostars and Te/BSA nanospheres to observe their cellular localization by confocal microscopy. After incubation with Te/BSA nanostars or Te/BSA nanospheres, the fluorescence images of MARC-145 cells were obtained by a confocal microscope. We found that both Te/BSA nanostars and Te/BSA nanospheres were distributed in the cytoplasm. Interestingly, the green fluorescence signal was remarkably higher in Te/BSA nanostar group than in Te/BSA nanosphere group (Fig. S7†), which supported our hypothesis. However, this conclusion needs to be confirmed by further experiments.

BSA is a common material used to synthesize nanoparticles due to its novel biological activity.[72,73] Especially, BSA-based nanomaterials are widely applied in biomedicine for their good properties of drug load. For example, doughnut-shaped BSA nanoparticles loaded with doxorubicin are utilized to overcome multidrug resistance during cancer treatment.[22] Therefore, it is a feasible strategy to improve the antiviral activity of Te/BSA nanostars by loading effective antiviral drugs.

3. Conclusions

In our study, the prepared Te/BSA nanostars were found to have excellent antiviral properties against arteriviruses with PRRSV as a virus model. Detailed study demonstrated that Te/BSA nanostars repressed the adsorption, internalization and replication stages of PRRSV infection, but had no inhibitory effect on the virion release process. Interestingly, Te/BSA nanostars significantly reduced PRRSV-induced intracellular ROS production, which might contribute to their antiviral activity. Moreover, the antiviral effect of Te/BSA nanostars on coronaviruses was also proved using PEDV as a model, suggesting the broad antiviral spectrum of Te/BSA nanostars. The overall results indicate that Te/BSA nanostar is a potential novel material for the development of antiviral strategy in the future.

4. Experimental section

4.1 Antiviral assay

Cells were treated with materials (Te/BSA nanostars, Te/BSA nanospheres, Te/BSA@MES nanospheres or MES) in DMEM (2% FBS) at 37 °C for 2 h. Meanwhile, virus was preincubated with the corresponding materials at 4 °C for 1 h. Then the above mixture of virus and materials was added to the pretreated cells, and incubated for 1 h at 37 °C. After two washes with serum-free DMEM to remove non-internalized virions, the cells were cultured with the materials in DMEM (2% FBS) for preset time.

4.2 One-step growth curve of PRRSV

MARC-145 cells were treated with Te/BSA nanostars (15.0 μg mL^{-1}) and PRRSV (MOI = 1.0) as described in Antiviral assay. Then one-step growth curves were established by viral plaque assays to test the titers of PRRSV in cell and supernatant at 12, 24, 36 and 48 hpi, respectively.[33]

4.3 Adsorption assay

Cells were pre-cooled at 4 °C for 30 min, then infected with PRRSV (0.001 and 0.0001 MOI) in the presence or absence of Te/BSA nanostars (15.0 μg mL^{-1}) at 4 °C for 2 h to permit adsorption. The excess Te/BSA nanostars and non-adsorbed PRRSV were removed by washing twice with precooling serum-free DMEM. Finally, low melting point agarose was added to the cells as described in viral plaque assay, followed by incubation at 37 °C under 5% CO_2 for a further two days to detect the plaque number.

4.4 Internalization assay

Cells were pre-cooled at 4 °C for 30 min, followed by infection with PRRSV (0.0001 MOI) for another 2 h at 4 °C. Next, the non-adsorbed PRRSV was removed by washing twice with precooling serum-free DMEM, and the cells were incubated with fresh DMEM or DMEM containing Te/BSA nanostars (15.0 μg mL^{-1}) at 37 °C for 3 h to allow viral internalization. After two washes with precooling serum-free DMEM to remove the non-internalized virions and excess Te/BSA nanostars, low melting point agarose was added to the cells as described in viral plaque assay. Plaques were counted after about 48 h.

4.5 Replication assay

MARC-145 cells were infected with PRRSV (1.0 MOI), then the supernatant was substituted with fresh DMEM (2% FBS) containing or not containing Te/BSA nanostars (15.0 μg mL^{-1}) at 6 hpi. After incubation for additional 1, 2, 3 and 4 h, the effect of

Te/BSA nanostars on PRRSV replication was assessed through detecting PRRSV negative-strand RNA levels by RT-qPCR assay.

4.6 Virion release assay

Cells were infected with PRRSV (1.0 MOI) and incubated for 18 h, then the cells were cultured in fresh medium with or without 15.0 μg mL^{-1} Te/BSA nanostars. After incubation for another 15, 30, 45 and 60 min, the titers of supernatant PRRSV and cellular PRRSV were detected by viral plaque assays, respectively.

4.7 Inactivation assay

PRRSV was preincubated or mock preincubated with Te/BSA nanostars at different concentrations (3.75, 7.50, and 15.0 μg mL^{-1}) at 4 °C for 1 h. Simultaneously, cells were pre-cooled at 4 °C for 30 min. Then the cells were incubated with the pre-treated PRRSV at 4 °C for another 2 h. After washing with pre-cooling serum-free DMEM to remove non-adsorbed PRRSV and excess Te/BSA nanostars, low melting point agarose was added to the cells as described in viral plaque assay. The titer of PRRSV was evaluated by the number of virus plaque.

4.8 Cell pretreatment assay

Cells were incubated or mock-incubated with Te/BSA nanostars (15.0 μg mL^{-1}) in DMEM (2% FBS) at 37 °C for 2 h. Then the cells were infected with PRRSV (1.0 MOI) at 37 °C for another 36 h. Virus titers were detected by viral plaque assay.

4.9 Measurement of the production of reactive oxygen species (ROS)

The levels of ROS were tested with ROS kit (DCFH-DA). Cells were incubated with Te/BSA nanostars (15.0 μg mL^{-1}) and PRRSV (1.0 MOI) as described in Antiviral assay. At 36 hpi, the cells were incubated with DCFH-DA, which was diluted at 1 : 2000 to give a final concentration of 5.00 μmol L^{-1}. After 0.5 h, the supernatant was substituted with Opti-MEM. The fluorescence images were obtained with an inverted fluorescence microscope.

To relatively quantify the intracellular ROS levels, cells treated as described above were washed twice with Opti-MEM, and then digested to single cells with 0.06% trypsin, followed by terminating the digestion reaction with DMEM (2% FBS). After two washes with PBS combined with centrifugation at 2000 rpm for 5 min, the ROS levels were evaluated by measuring the relative fluorescence intensity with a flow cytometer.

Conflicts of interest

There are no conflicts to declare.

Acknowledgements

This work was supported by the National Natural Sciences Foundation of China (31490602, 31772785), the National Basic Research Program (973) of China (2014CB542700), and the Special Project for Technology Innovation of Hubei Province (2017ABA138).

References

1 O. Adegoke, M. W. Seo, T. Kato, S. Kawahito and E. Y. Park, *J. Mater. Chem. B*, 2016, **4**, 1489–1498.
2 X. X. Yang, C. M. Li and C. Z. Huang, *Nanoscale*, 2016, **8**, 3040–3048.
3 I. Donskyi, M. Druke, K. Silberreis, D. Lauster, K. Ludwig, C. Kuhne, W. Unger, C. Bottcher, A. Herrmann, J. Dernedde, M. Adeli and R. Haag, *Small*, 2018, **14**, e1800189.
4 D. Lauster, M. Glanz, M. Bardua, K. Ludwig, M. Hellmund, U. Hoffmann, A. Hamann, C. Boettcher, R. Haag, C. P. R. Hackenberger and A. Herrmann, *Angew. Chem., Int. Ed. Engl.*, 2017, **56**, 5931–5936.
5 A. Riegger, C. Chen, O. Zirafi, N. Daiss, D. Mukherji, K. Walter, Y. Tokura, B. Stoeckle, K. Kremer, F. Kirchhoff, D. Y. W. Ng, P. C. Hermann, J. Muench and T. Weil, *ACS Macro Lett.*, 2017, **6**, 241–246.
6 A. Haider, S. Das, D. Ojha, D. Chattopadhyay and A. Mukherjee, *Mater. Sci. Eng., C*, 2018, **89**, 413–421.
7 B. Villeret, A. Dieu, M. Straube, B. Solhonne, P. Miklavc, S. Hamadi, R. Le Borgne, A. Mailleux, X. Norel, J. Aerts, D. Diallo, F. Rouzet, P. Dietl, J. M. Sallenave and I. Garcia-Verdugo, *ACS Nano*, 2018, **12**, 1188–1202.
8 H. Liu, Y. Bai, Y. Zhou, C. Feng, L. Liu, L. Fang, J. Liang and S. Xiao, *RSC Adv.*, 2017, **7**, 28016–28023.
9 S. Huang, J. Gu, J. Ye, B. Fang, S. Wan, C. Wang, U. Ashraf, Q. Li, X. Wang, L. Shao, Y. Song, X. Zheng, F. Cao and S. Cao, *J. Colloid Interface Sci.*, 2019, **542**, 198–206.
10 A. Loczechin, K. Seron, A. Barras, E. Giovanelli, S. Belouzard, Y.-T. Chen, N. Metzler-Nolte, R. Boukherroub, J. Dubuisson and S. Szunerits, *ACS Appl. Mater. Interfaces*, 2019, **11**, 42964–42974.
11 X. D. Zhang, Z. Luo, J. Chen, H. Wang, S. S. Song, X. Shen, W. Long, Y. M. Sun, S. Fan, K. Zheng, D. T. Leong and J. Xie, *Small*, 2015, **11**, 1683–1690.
12 Y. S. Kim, M. Y. Song, J. D. Park, K. S. Song, H. R. Ryu, Y. H. Chung, H. K. Chang, J. H. Lee, K. H. Oh, B. J. Kelman, I. K. Hwang and I. J. Yu, *Part. Fibre Toxicol.*, 2010, **7**, 20.
13 J. Zou, H. Feng, M. Mannerstrom, T. Heinonen and I. Pyykko, *J. Nanobiotechnol.*, 2014, **12**, 52.
14 V. Cagno, P. Andreozzi, M. D'Alicarnasso, P. Jacob Silva, M. Mueller, M. Galloux, R. Le Goffic, S. T. Jones, M. Vallino, J. Hodek, J. Weber, S. Sen, E. R. Janecek, A. Bekdemir, B. Sanavio, C. Martinelli, M. Donalisio, M. A. Rameix Welti, J. F. Eleouet, Y. Han, L. Kaiser, L. Vukovic, C. Tapparel, P. Kral, S. Krol, D. Lembo and F. Stellacci, *Nat. Mater.*, 2018, **17**, 195–203.
15 L. Rodriguez-Perez, J. Ramos-Soriano, A. Perez-Sanchez, B. M. Illescas, A. Munoz, J. Luczkowiak, F. Lasala, J. Rojo, R. Delgado and N. Martin, *J. Am. Chem. Soc.*, 2018, **140**, 9891–9898.

16 V. Cagno, M. Donalisio, A. Civra, M. Volante, E. Veccelli, P. Oreste, M. Rusnati and D. Lembo, *Antimicrob. Agents Chemother.*, 2014, **58**, 4782–4794.
17 D. Baram-Pinto, S. Shukla, N. Perkas, A. Gedanken and R. Sarid, *Bioconjugate Chem.*, 2009, **20**, 1497–1502.
18 D. Baram-Pinto, S. Shukla, A. Gedanken and R. Sarid, *Small*, 2010, **6**, 1044–1050.
19 P. Dey, T. Bergmann, J. L. Cuellar-Camacho, S. Ehrmann, M. S. Chowdhury, M. Zhang, I. Dahmani, R. Haag and W. Azab, *ACS Nano*, 2018, **12**, 6429–6442.
20 A. R. Deokar, A. P. Nagvenkar, I. Kalt, L. Shani, Y. Yeshurun, A. Gedanken and R. Sarid, *Bioconjugate Chem.*, 2017, **28**, 1115–1122.
21 B. Ziem, J. Rahn, I. Donskyi, K. Silberreis, L. Cuellar, J. Dernedde, G. Keil, T. C. Mettenleiter and R. Haag, *Macromol. Biosci.*, 2017, **17**, 1600499.
22 Z. Kayani, O. Firuzi and A. K. Bordbar, *Int. J. Biol. Macromol.*, 2018, **107**, 1835–1843.
23 N. Doshi and S. Mitragotri, *PLoS One*, 2010, **5**, e10051.
24 S. S. Justice, D. A. Hunstad, L. Cegelski and S. J. Hultgren, *Nat. Rev. Microbiol.*, 2008, **6**, 162–168.
25 E. A. Simone, T. D. Dziubla and V. R. Muzykantov, *Expert Opin. Drug Delivery*, 2008, **5**, 1283–1300.
26 G. Maiorano, L. Rizzello, M. A. Malvindi, S. S. Shankar, L. Martiradonna, A. Falqui, R. Cingolani and P. P. Pompa, *Nanoscale*, 2011, **3**, 2227–2232.
27 J. Ji, W. Zhu, J. Li, P. Wang, Y. Liang, W. Zhang, X. Yin, B. Wu and G. Li, *ACS Appl. Mater. Interfaces*, 2017, **9**, 19124–19134.
28 S. Zhu, A. G. Huang, F. Luo, J. Li, J. Li, L. Zhu, L. Zhao, B. Zhu, F. Ling and G. X. Wang, *ACS Appl. Mater. Interfaces*, 2019, **11**, 19006–19016.
29 S. Ye, K. Shao, Z. Li, N. Guo, Y. Zuo, Q. Li, Z. Lu, L. Chen, Q. He and H. Han, *ACS Appl. Mater. Interfaces*, 2015, **7**, 21571–21579.
30 Y. Si, Z. Zhang, W. Wu, Q. Fu, K. Huang, N. Nitin, B. Ding and G. Sun, *Sci. Adv.*, 2018, **4**, eaar5931.
31 Z. Lin, Y. Li, M. Guo, M. Xiao, C. Wang, M. Zhao, T. Xu, Y. Xia and B. Zhu, *RSC Adv.*, 2017, **7**, 35290–35296.
32 J. Vonnemann, C. Sieben, C. Wolff, K. Ludwig, C. Bottcher, A. Herrmann and R. Haag, *Nanoscale*, 2014, **6**, 2353–2360.
33 M. C. Rahe and M. P. Murtaugh, *Viruses*, 2017, **9**, 148.
34 Y. W. Huang and X. J. Meng, *Virus Res.*, 2010, **154**, 141–149.
35 E. Duan, D. Wang, L. Fang, J. Ma, J. Luo, H. Chen, K. Li and S. Xiao, *Antiviral Res.*, 2015, **120**, 122–125.
36 Q. Zhang and D. Yoo, *Vet. Microbiol.*, 2015, **177**, 229–241.
37 E. de Wit, N. van Doremalen, D. Falzarano and V. J. Munster, *Nat. Rev. Microbiol.*, 2016, **14**, 523–534.
38 J. F. Chan, S. Yuan, K. H. Kok, K. K. To, H. Chu, J. Yang, F. Xing, J. Liu, C. C. Yip, R. W. Poon, H. W. Tsoi, S. K. Lo, K. H. Chan, V. K. Poon, W. M. Chan, J. D. Ip, J. P. Cai, V. C. Cheng, H. Chen, C. K. Hui and K. Y. Yuen, *Lancet*, 2020, **395**, 514–523.
39 Y. Zhou, Y. Bai, H. Liu, X. Jiang, T. Tong, L. Fang, D. Wang, Q. Ke, J. Liang and S. Xiao, *ACS Appl. Mater. Interfaces*, 2018, **10**, 25241–25251.
40 J. C. Li, R. Cai, N. Kawazoe and G. P. Chen, *J. Mater. Chem. B*, 2015, **3**, 5806–5814.
41 X. Hu, X. An and L. Li, *Mater. Sci. Eng., C*, 2016, **58**, 730–736.
42 A. Talib, S. Pandey, M. Thakur and H. F. Wu, *Mater. Sci. Eng., C*, 2015, **48**, 700–703.
43 Y. Wang, S. Kalytchuk, Y. Zhang, H. Shi, S. V. Kershaw and A. L. Rogach, *J. Phys. Chem. Lett.*, 2014, **5**, 1412–1420.
44 Y. Zuo, T. Li, D. Rao, X. Lei, Q. Li, G. Zhu, R. Lu and H. Han, *J. Phys. Chem. C*, 2016, **120**, 12305–12312.
45 M. Lestelius, B. Liedberg and P. Tengvall, *Langmuir*, 1997, **13**, 5900–5908.
46 X. Q. Zou, H. F. Bao, H. W. Guo, L. Zhang, Q. Li, J. G. Jiang, L. Niu and S. J. Dong, *J. Colloid Interface Sci.*, 2006, **295**, 401–408.
47 E. Ieva, A. Trapani, N. Cioffi, N. Ditaranto, A. Monopoli and L. Sabbatini, *Anal. Bioanal. Chem.*, 2009, **393**, 207–215.
48 D. Zhang, X. Zhang, Y. Chen, C. Wang and Y. Ma, *Electrochim. Acta*, 2012, **69**, 364–370.
49 P. Wu, Y. Qian, P. Du, H. Zhang and C. Cai, *J. Mater. Chem.*, 2012, **22**, 6402–6412.
50 Z. Luo, S. Lim, Z. Tian, J. Shang, L. Lai, B. MacDonald, C. Fu, Z. Shen, T. Yu and J. Lin, *J. Mater. Chem.*, 2011, **21**, 8038–8044.
51 Y. N. Yu, M. Q. Wang and S. J. Bao, *J. Solid State Electrochem.*, 2017, **21**, 103–110.
52 E. K. Kim, D. Park, N. K. Shrestha, J. Chang, C. W. Yi and S. H. Han, *Dalton Trans.*, 2016, **45**, 17312–17318.
53 N. Li, B. Zhao, S. Zhou, S. Lou and Y. Wang, *Mater. Lett.*, 2012, **81**, 212–214.
54 Z. Shen, C. Luo, R. Huang, Y. Wang, H. Peng and J. Travas-Sejdic, *J. Lumin.*, 2014, **153**, 203–209.
55 H. Nosrati, N. Sefidi, A. Sharafi, H. Danafar and H. K. Manjili, *Bioorg. Chem.*, 2018, **76**, 501–509.
56 H. Jin, L. Zhou, X. Ge, H. Zhang, R. Zhang, C. Wang, L. Wang, Z. Zhang, H. Yang and X. Guo, *Virus Res.*, 2017, **238**, 204–212.
57 D. Sepulveda-Crespo, R. Cena-Diez, J. L. Jimenez and M. Angeles Munoz-Fernandez, *Med. Res. Rev.*, 2017, **37**, 149–179.
58 X. X. Yang, C. M. Li, Y. F. Li, J. Wang and C. Z. Huang, *Nanoscale*, 2017, **9**, 16086–16092.
59 S. Ye, K. Shao, Z. Li, N. Guo, Y. Zuo, Q. Li, Z. Lu, L. Chen, Q. He and H. Han, *ACS Appl. Mater. Interfaces*, 2015, **7**, 21571–21579.
60 D. G. Yoo, M. C. Kim, M. K. Park, J. M. Song, F. S. Quan, K. M. Park, Y. K. Cho and S. M. Kang, *J. Med. Food*, 2012, **15**, 855–862.
61 D. Xiang, Y. Zheng, W. Duan, X. Li, J. Yin, S. Shigdar, M. L. O'Connor, M. Marappan, X. Zhao, Y. Miao, B. Xiang and C. Zheng, *Int. J. Nanomed.*, 2013, **8**, 4103–4113.
62 Y. Y. Huang, Y. Luo, W. J. Zheng and T. F. Chen, *ACS Appl. Mater. Interfaces*, 2014, **6**, 19217–19228.
63 Y. Li, Z. Lin, M. Zhao, T. Xu, C. Wang, L. Hua, H. Wang, H. Xia and B. Zhu, *ACS Appl. Mater. Interfaces*, 2016, **8**, 24385–24393.
64 H. O. Kim, M. Yeom, J. Kim, A. Kukreja, W. Na, J. Choi, A. Kang, D. Yun, J. W. Lim, D. Song and S. Haam, *Small*, 2017, **13**, 1700818.
65 Y. Li, Z. Lin, M. Guo, M. Zhao, Y. Xia, C. Wang, T. Xu and B. Zhu, *Int. J. Nanomed.*, 2018, **13**, 2005–2016.

66 M. L. Reshi, Y. C. Su and J. R. Hong, *Int. J. Cell Biol.*, 2014, **2014**, 467452.
67 M. C. Bowman, T. E. Ballard, C. J. Ackerson, D. L. Feldheim, D. M. Margolis and C. Melander, *J. Am. Chem. Soc.*, 2008, **130**, 6896–6897.
68 A. K. Lytton-Jean and C. A. Mirkin, *J. Am. Chem. Soc.*, 2005, **127**, 12754–12755.
69 D. Wang, L. Fang and S. Xiao, *Virus Res.*, 2016, **226**, 7–13.
70 C. C. Huan, Y. Wang, B. Ni, R. Wang, L. Huang, X. F. Ren, G. Z. Tong, C. Ding, H. J. Fan and X. Mao, *Arch. Virol.*, 2015, **160**, 1621–1628.
71 P. S. Kwon, S. Ren, S. J. Kwon, M. E. Kizer, L. Kuo, M. Xie, D. Zhu, F. Zhou, F. Zhang, D. Kim, K. Fraser, L. D. Kramer, N. C. Seeman, J. S. Dordick, R. J. Linhardt, J. Chao and X. Wang, *Nat. Chem.*, 2020, **12**, 26–35.
72 C. Ding, Y. Xu, Y. Zhao, H. Zhong and X. Luo, *ACS Appl. Mater. Interfaces*, 2018, **10**, 8947–8954.
73 A. Zhang, W. Guo, H. Ke, X. Zhang, H. Zhang, C. Huang, D. Yang, N. Jia and D. Cui, *Biosens. Bioelectron.*, 2018, **101**, 219–226.